Supporting information

Insight into the Boosted Electrocatalytic Oxygen Evolution Performance of Highly Hydrophilic Nickel-iron Hydroxide

*Yi Wei, Cheol-Hwan Shin, Emmanuel Batsa Tetteh, Byong-June Lee and Jong-Sung Yu**

Department of Energy Science and Engineering, Daegu Gyeongbuk Institute of Science and Technology (DGIST), Daegu 42988, Republic of Korea.

Corresponding Author:

(J.-S. Yu) E-mail: jsyu@dgist.ac.kr.

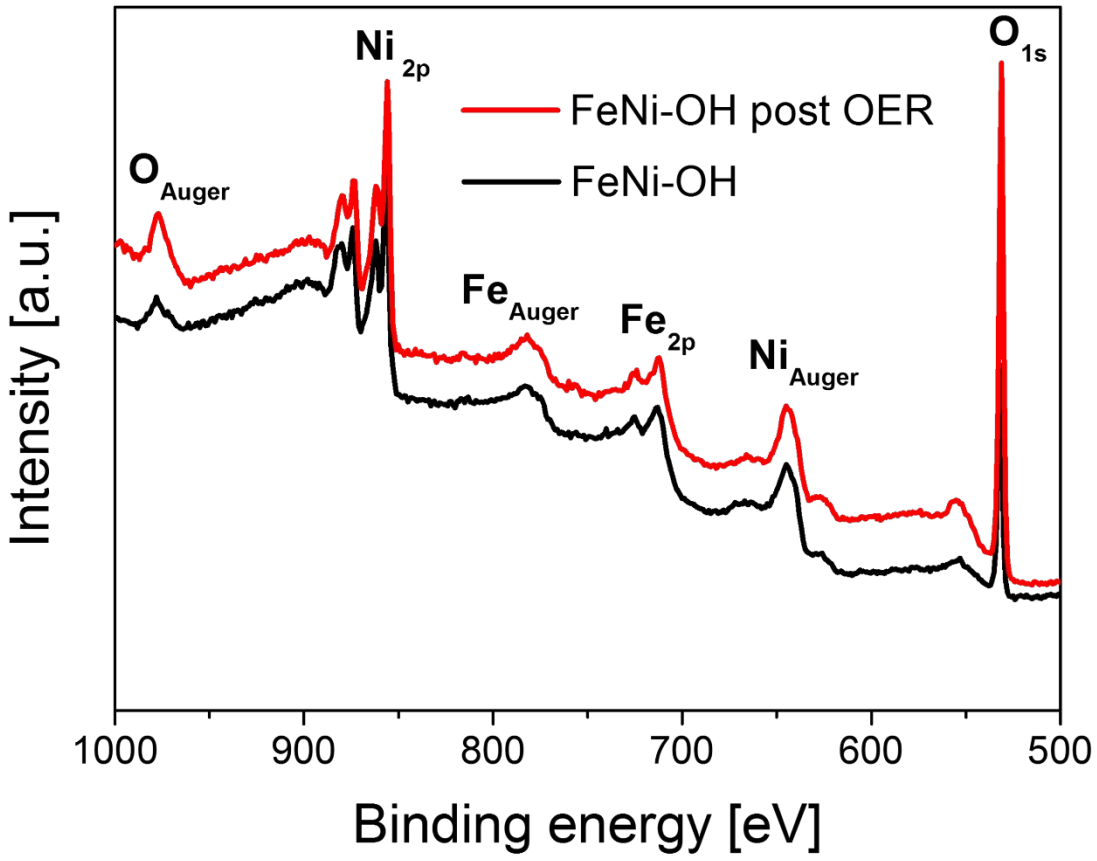

Figure S1. XPS survey spectra of NiFe-OH before and after the OER reaction performed in Figure 3c.

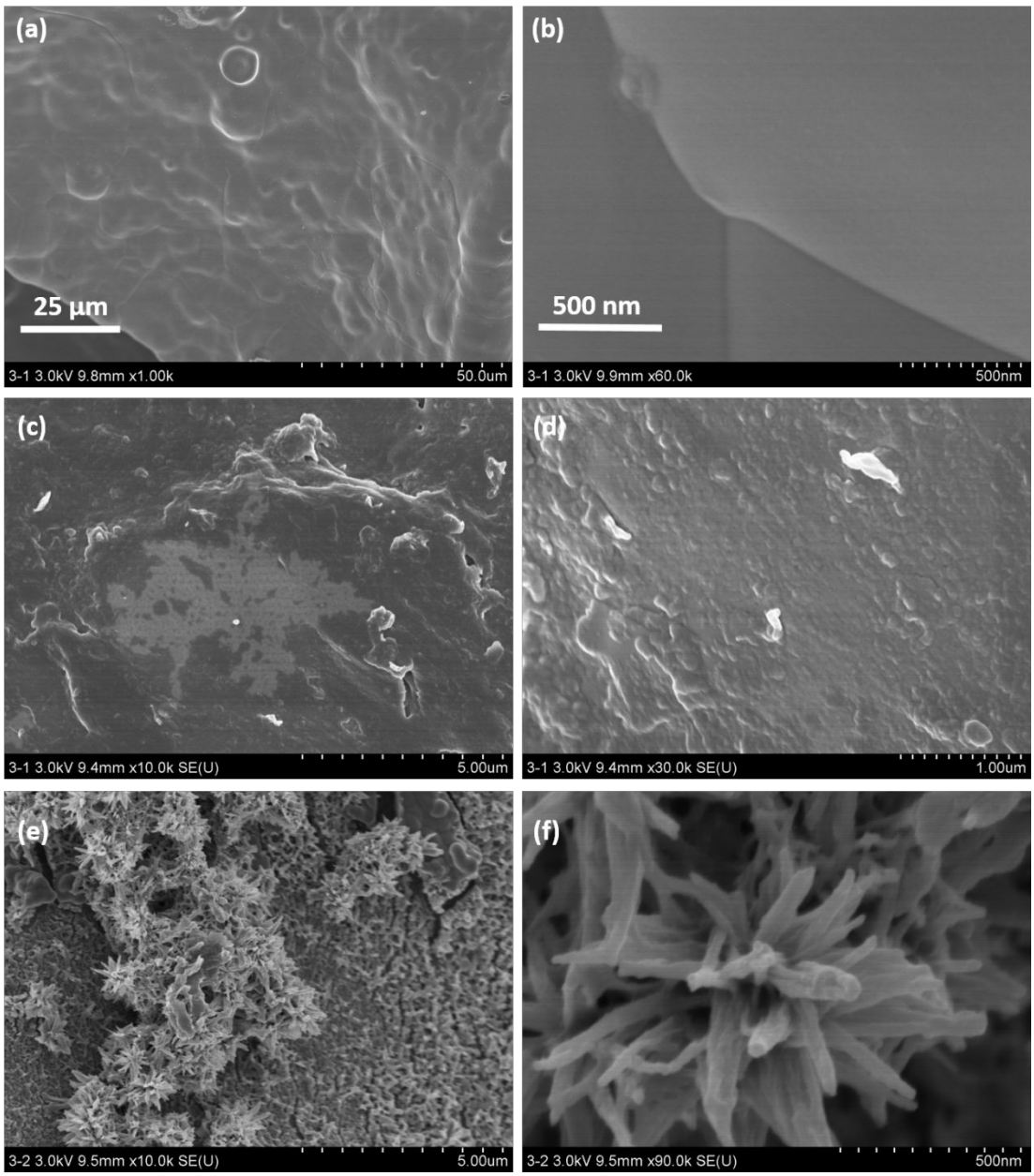

Figure S2. SEM images of (a) and (b) bare nickel foam (NF), (c) and (d) Ni-OH/NF, and (e) and (f) Fe-OH/NF.

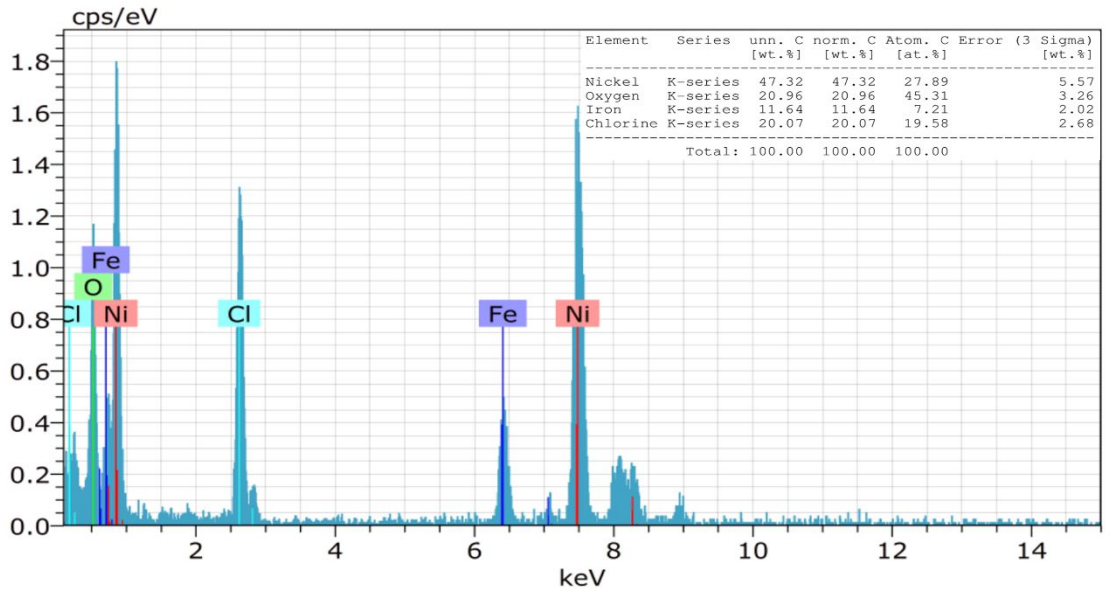

Figure S3. Energy-dispersive X-ray spectroscopy (EDS) spectrum on the chemical compositions of NiFe-OH.

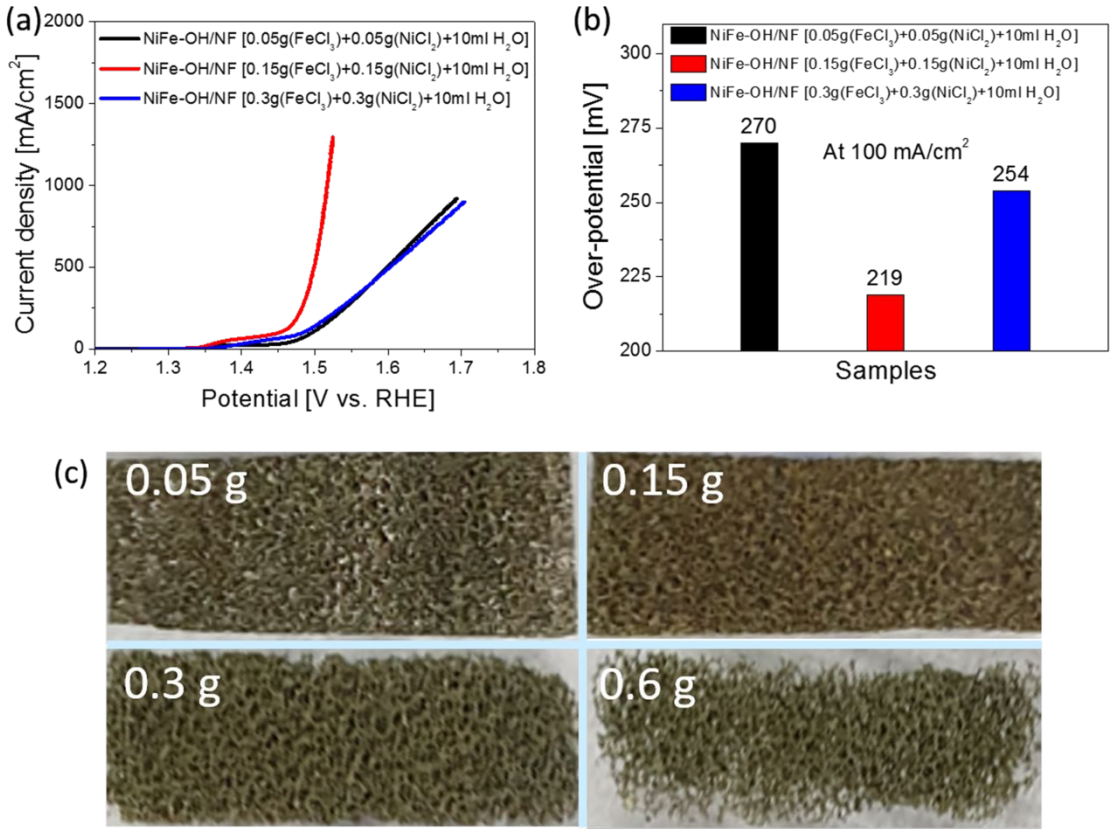

Figure S4. (a) Steady-state polarization curves of the OER activity (with iR-correction), (b) overpotential profiles at 100 mA/cm^2 and (c) photographic images of NiFe-OH/NF samples prepared with different precursor concentrations of Ni^{2+} and Fe^{3+} in the synthesis.

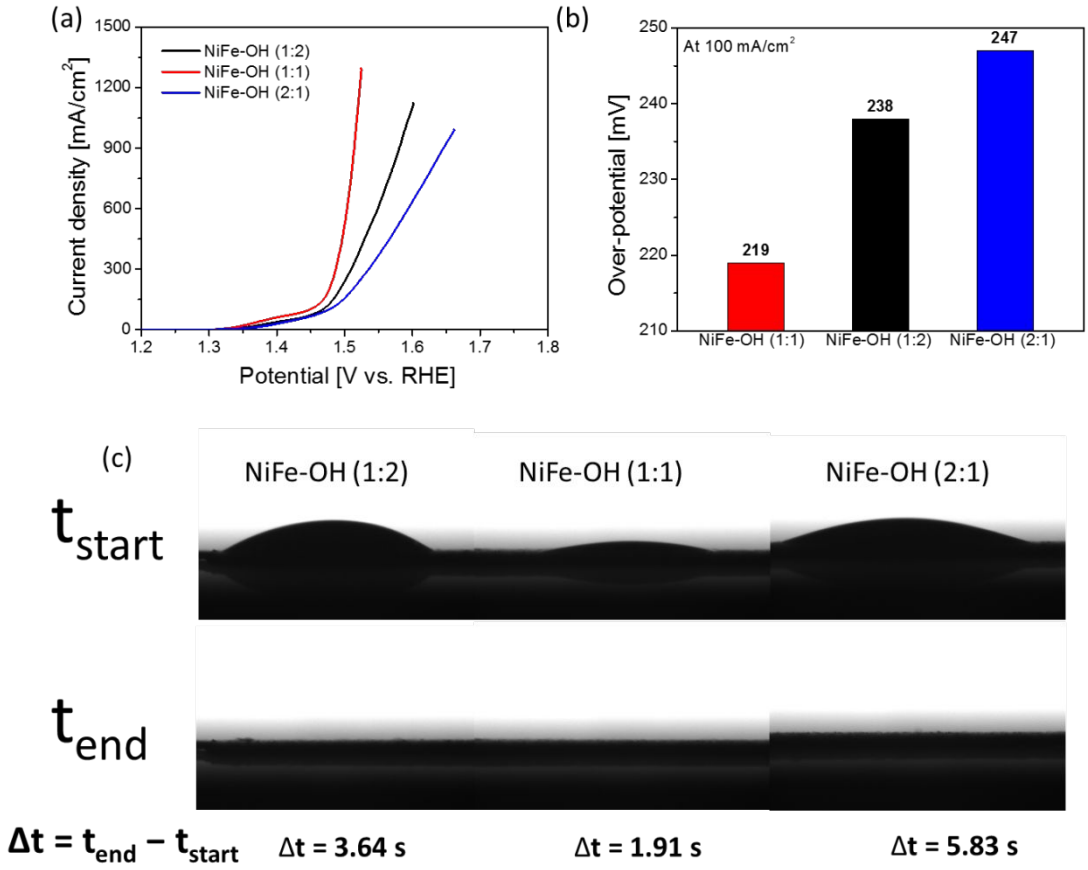

Figure S5. (a) The effect of different relative ratios in amount used between $NiCl_2$ and $FeCl_3$ on steady-state polarization curves of the OER activity (with iR correction), and (b) corresponding overpotentials at 100 mA/cm^2. (c) The effect of the relative ratios on water contact angle in the corresponding FeNi-OH/NF samples.

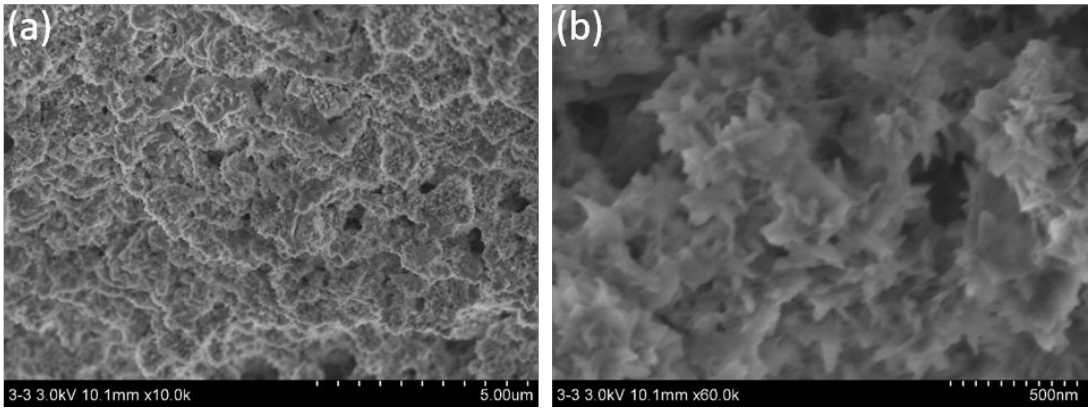

Figure S6. (a) and (b) SEM images of NiFe-OH/NF obtained after long-term OER stability test examined in Figure 3c.

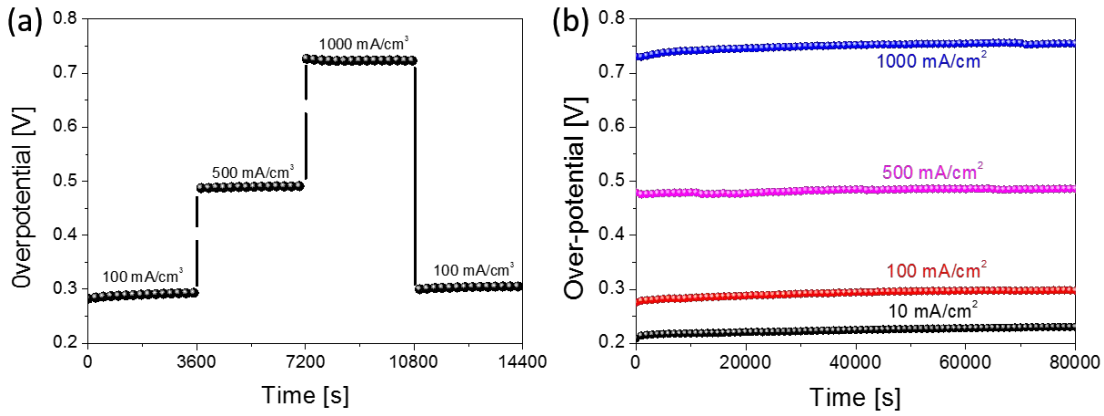

Figure S7. (a) Chronopotentiometric curve of NiFe-OH/NF at different current densities of 100, 500 and 1000 mA cm^{-2}, respectively and (b) long-term chronopotentiometric stability test profiles of the NiFe-OH/NF at each current density of 10, 100, 500, and 1000 mA cm^{-2} without IR correction.

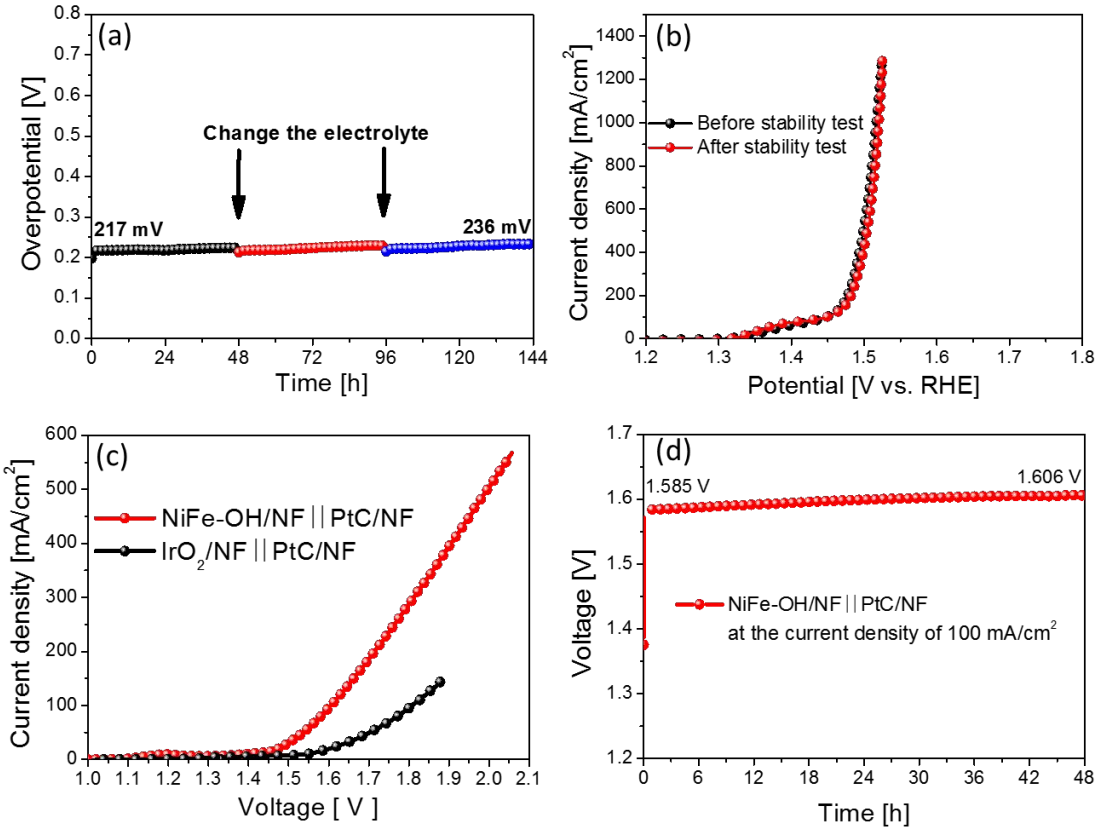

Figure S8. (a) Chronopotentiometric long-term stability analysis of the NiFe-OH/NF at a current density of 100 mA cm^{-2} for 6 days, (b) polarization curves of NiFe-OH/NF for OER before and after the chronopotentiometry analysis for 6 days, (c) full cell water-splitting performance of NiFe-OH/NF||PtC/NF and IrO_2/NF||PtC/NF and (d) stability test of the NiFe-OH/NF||PtC/NF at the current density of 100 mA cm^{-2} in 1.0 M KOH without iR correction.

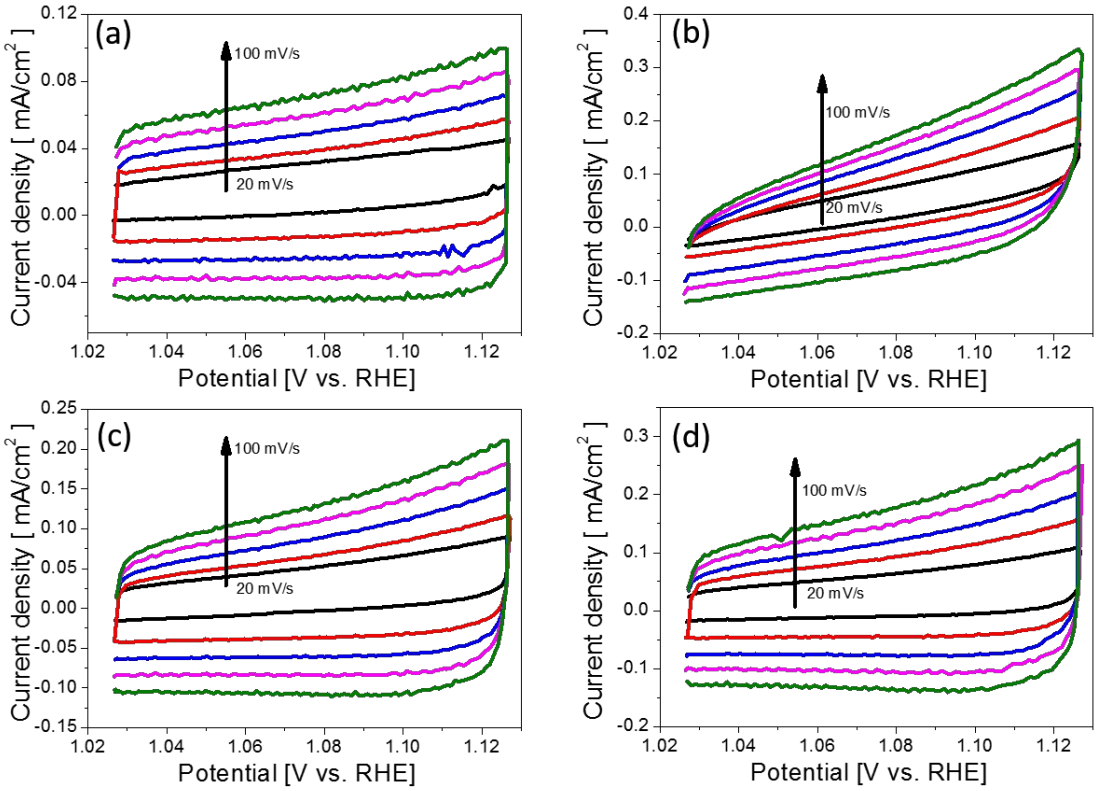

Figure S9. Cyclic voltammetry curves of (a) NF, (b) Ni-OH/NF, (c) Fe-OH/NF, and (d) NiFe-OH/NF at different scan rates from 20 to 100 mV s^{-1} with a 20 mV s^{-1} interval in the potential range from 1.024 V to 1.124 V vs RHE.

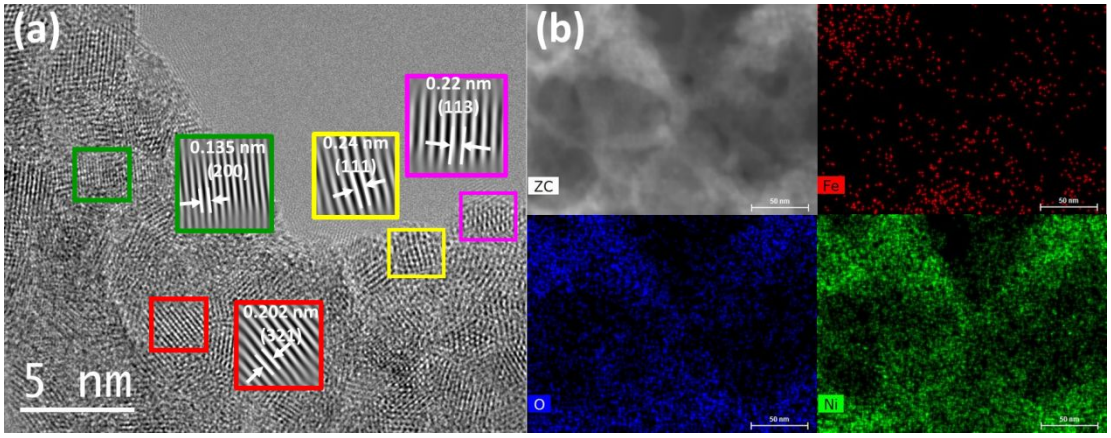

Figure S10. (a) HR-TEM image and (b) EDX element mapping images of the NiFe-OH obtained after the long-term stability test shown in Figure 3c.

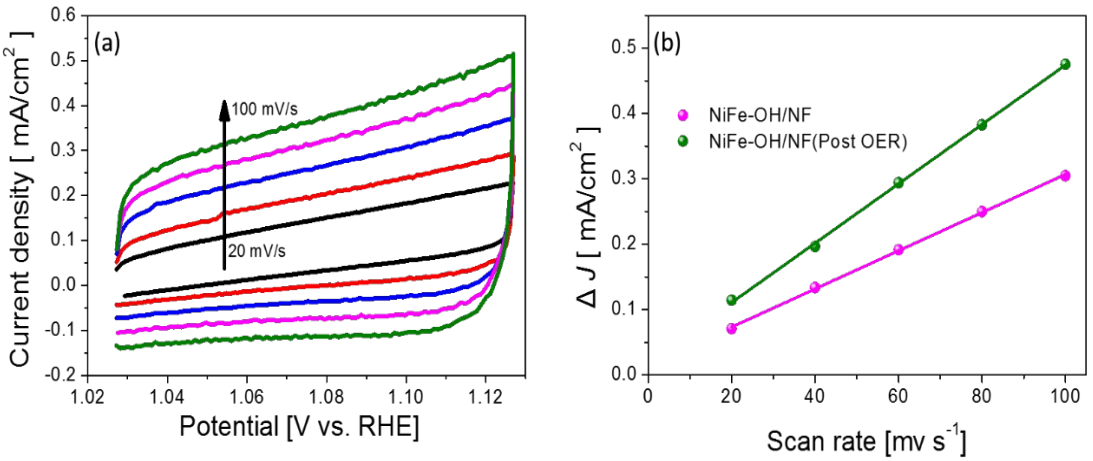

Figure S11. (a) Cyclic voltammetry curves of NiFe-OH/NF collected after the long-term OER stability test shown in Figure 3c at different rates from 20 to 100 mV s^{-1} with a 20 mV s^{-1} interval in the potential range from 1.024 V to 1.124 V vs RHE and (b) capacitive ΔJ ($= J_a - J_c$) versus the scan rates of the NiFe-OH/NF before and after the the OER stability test.